Benchmark Tests for Strong Ground Motion Prediction Methods Using Numerical Methods

Chiaki YOSHIMURA, Masayuki NAGANO, Yoshiaki HISADA
Osaka University, Japan, Tokyo University of Science, Japan, Kogakuin University, Japan

Shin AOI, Asako IWAKI
NIED, Japan

Takashi HAYAKAWA, Seckin Ozgur CITAK, Shinichi MATSUSHIMA
Shimizu Corporation, Japan, JAMSTEC, Japan, Kyoto University, Japan

Hidenori KAWABE, Hirotoshi UEBAYASHI, Yoshihiro ONISHI
Kyoto University, Japan

SUMMARY
We conducted a benchmark test with finite difference method (FDM) and finite element method (FEM). Total of 7 teams participated in and solved common problems with the same underground structure models and source models. During 3 years of the research period, we studied 14 problems categorized in 6 steps with various degree of complexity. In step 1, we studied a homogeneous model and a two-layer model with a point source. In step 2, we studied the two-layer model with extended source models (a lateral fault and a reverse fault). In step 3 and 4, we considered a four-layer model, a symmetric trapezoidal basin model and an asymmetric slant-basement basin model. In step 5 and 6, we studied a realistic Kanto basin model where Tokyo is located, simulating past observed earthquakes and 1923 Kanto earthquake.

Keywords: Finite difference method, Finite element method, Seismic source model, Kanto Basin

1. PARTICIPATING TEAMS AND METHODS

Table 1 summarizes participating teams during all steps and their methods. One team (Yoshimura) solved with FEM, and 6 teams (Aoi & Iwaki, Nagano, Hayakawa, Citak & Matsusihima & Graves, Onishi and Kawabe) solved with FDM. Uebayashi solved only Case N33 with Aki & Larner method for the purpose of comparison to boundary method. The table shows the references that each code bases on. Regarding grid space of FDM, those of Aoi & Iwaki, Nagano and Kawabe are variable both in horizontal directions and in vertical direction. Those of Hayakawa and Onishi are fixed horizontally and variable vertically. That of Citak et al. are fixed horizontally and vertically. Yoshimura's FEM varied element size in each layer. The effect of grid space came to an issue when the allocation of soil properties near the surface were concerned in step 5 and 6. The table shows the ways to introduce absorbing boundary, absorbing zone and material damping. All teams used Q value proportional to frequency except that Citak used constant Q.

2. STEP1, 2 (HOMOGENEOUS MEDIA, TWO-LAYERED MEDIA)

In step 1 and 2, we started with simple subsurface ground structure and source models following Day et al.(2000) and Day et al.(2003). Table 2 summarizes test cases. For N11 we considered a homogeneous media, and for N12 and N13 a two-layered media. Only for N13 we considered internal damping of the soil, and for other models we set Q value to be infinity. In step 2, we considered the two-layered model and extended sources: a vertical lateral fault and a low-angle reverse fault.

Figure 1(a) shows the fourth part of the calculation domain for N11 and figure 1(b) for N12 and N13. Cartesian coordinates are set such that +X is north, +Y is east and +Z is downward. Model size is 30km x 30km x 17 km (-15< X < 15, -15 < Y < 15, -17 < Z < 0 (km)) except absorbing zone. Each participant adds necessary absorbing zone at model sides and the bottom. Table 3 shows the soil properties for the homogeneous model (N11), the two layered model without internal damping (N12, N21 and N22) and with damping (N13).

Table 1. Participating teams and their methods

Team	Yoshimura	Aoi & Iwaki	Nagano	Hayakawa	Citak, Matsushima and Graves	Onishi	Kawabe	Uebayashi
Method	FEM	FDM						AL
Reference	Bao et al.(1998)	Aoi and Fujiwara (1999)	Nagano (2004)	Pitarka (1999)	Graves(1996) Graves and Day(2003)	Graves(1996) Pitarka(1999)	Pitarka(1999)	Uebayashi et al.(1992)
Grid space Horizontal Vertical	–	variable variable	variable variable	fixed variable	fixed fixed	fixed variable	variable variable	–
Absorbing boundary	Lysmer and Kuhlemeyer (1969)	Clayton and Engquist (1977)	Clayton and Engquist (1977)	Clayton and Engquist (1977)	Clayton and Engquist (1977)	Clayton and Engquist (1977)	Clayton and Engquist (1977)	Satisfy radiation condition at infinity
Q value at absorbing zone	Same as calculation domain	Cerjan et al. (1985)	gradsual increase Q=5 to 50	Q=25	gradual increase Q=5 to 50		Cerjan et al. (1985)	
Material damping	Mass proportional damping	Graves(1996)	Graves(1996)	Graves(1996)	Graves and Day (2003)	Graves(1996)	Graves(1996)	Introduce to imaginary part of P and S velocity
	Q is proportional to frequency				constant Q	Q is proportional to frequency		
Step 1, 2	O	O	O	O	O	O	–	–
Step 3, 4	O	O	O	O	O	–	O	O (N33)
Step 5, 6	O	O	O	O	O	–	O	–

Table 2. Test cases of Step 1 and 2

Case	N11	N12	N13	N21	N22
Media	homogeneous	two-layered			
Internal damping	NO	YES	NO		
Source	point source			lateral fault	reverse fault
Effective frequency	0 – 5 Hz				
Calculation points	−10〜10 km(21 points with 1km interval)				
Reference models Day et al. (2000)	UHS.1 UHS.2	LOH.1	LOH.3	LOH.2	LOH.4

Table 3. Material properties

Case	Layer	Thickness D (m)	P wave velocity Vp (m/s)	S wave velocity Vs (m/s)	Density ρ (kg/m^3)	Q Value Qp	Qs
N11	–	–	6000	3464	2700	infinity	infinity
N12, N21, N22	upper	1000	4000	2000	2600	infinity	infinity
	lower	–	6000	3464	2700	infinity	infinity
N13	upper	1000	4000	2000	2600	40f	40f
	lower	–	6000	3464	2700	70f	70f

f: frequency (Hz)

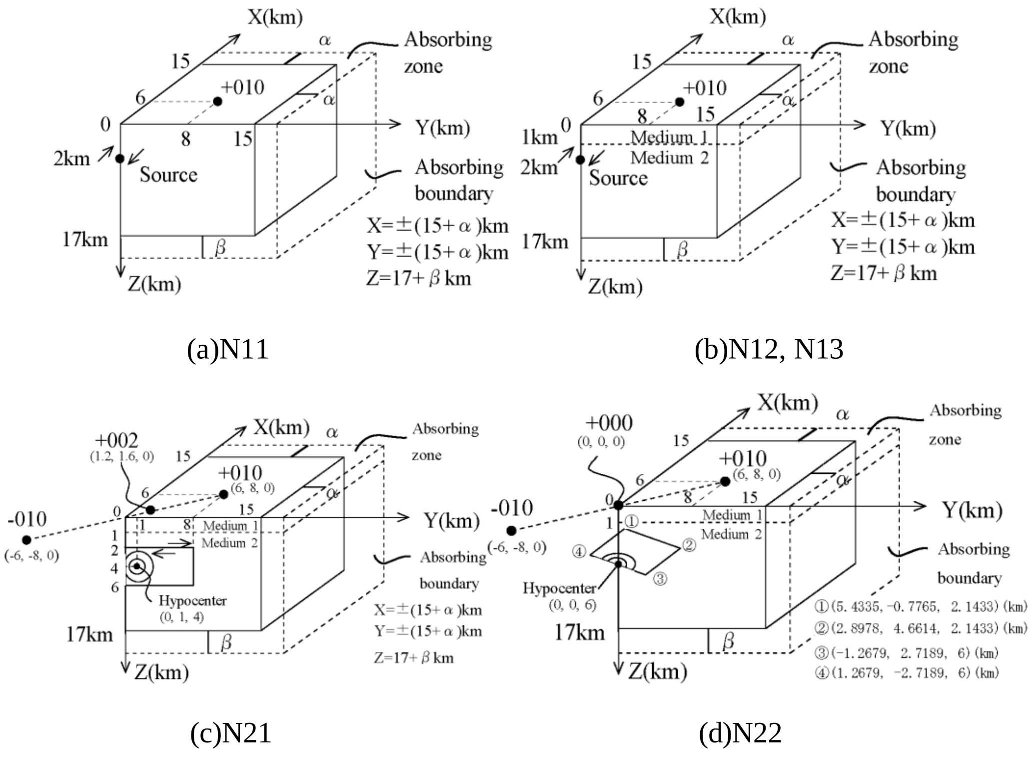

Figure 1. Fourth part of calculation domain and source model

A double couple point source is located at the center of the model with the depth of 2km, or (X,Y,Z) = (0, 0, 2)(km). Moment magnitude Mo is set to be 10^{18} Nm. Only M_{xy} ($=M_{yx}$) of moment tensor is non-zero. Moment function *M(t)*, moment rate function $\dot{M}(t)$ are given by eq. (1), (2) respectively.

$$M(t) = M_0 \cdot (1 - (1 + \frac{t}{T}) \cdot e^{-\frac{t}{T}}) \qquad (1)$$

$$\dot{M}(t) = M_0 \cdot \frac{t}{T^2} \cdot e^{-\frac{t}{T}} \qquad (2)$$

Where t denotes time(s), T is a constant (=0.1s), and e is the base of natural logarithm.

Table 4 summarizes calculation condition of each team. Grid space for FDM and elements size for FEM were chosen so that the calculation is valid from 0 to 5 Hz in frequency. For example, fourth-order finite difference method requires 5 grids per wavelength, which leads to that it is valid up to f=6.9 Hz with H=100m spacing in bedrock of Vs=3464 (f=Vs/(5H)). The choice of soil properties at the boundary of upper layer and lower layer (Z=1km) varied among teams. Aoi & Iwaki chose those of upper layer. Nagano and Citak et al. chose average of upper layer and lower layer. Hayakawa and Onishi chose those of lower layer. Because Yoshimura's FEM allocates soil properties to elements, it gives better approximation than FDM. Division size of extended fault is 50m to 100m, which is comparable to grid size. It was chosen to be as dense as possible to express smooth rupture propagation. Participants submitted velocity time histories with time increment of 0.01s at 21 surface points (-010～+010) along the vector (X,Y,Z)=(0.6, 0.8, 0)(km) with 1km interval. Submitted velocity time histories were processed with a 5Hz low-pass filter.

Figure 2 shows the results of 6 teams for N11. Radial, Transverse and Up component of velocity at calculation point +010 (shown in Fig.1. Epicentral distance is 10km.) are compared. In addition, theoretical waveforms by Hisada's method (Hisada, 1994a, 1994b) are shown. The results of 6 teams show very good agreement to each other. The waveforms are very simple because of simple media and source. P wave arrival at 1.7 seconds in radial component and S wave arrival at 2.9 seconds in transverse component are obviously recognized.

Figure 3 shows the results of N12. Radial component at +010 are shown. The shape and amplitude show good agreement among teams, yet slight differences of phase arrival are recognized. The initial phase at 2 seconds are identical among teams. As time increase, the arrival time of peaks become earlier. For example, Hisada's theoretical result have dominant peak at 4.57 seconds. The corresponding peak of Aoi's result arrives 0.02 seconds earlier. Similarly, Nagano's peak arrives 0.01s earlier, Yoshimura's 0.01s, Citak's 0.05s, Hayakawa's 0.07s, and Onishi's 0.12s. The time lags of Hayakawa and Onishi is large. The reason may be that Hayakawa and Onishi give the soil properties of basement at the grids on the boundary of upper layer and lower layer. Figure 4 shows the results of N13. Radial component at +010 are shown. Internal damping is introduced to the same model as N12. The amplitude of waveforms becomes about 80% of N12. Because the waveforms of all teams show as good agreement as N12, it seems that internal damping is introduced successfully by all teams. The amplitude of Citak's result is smaller than other teams because Citak uses constant Q.

Table 4. Calculation condition of each team

			Yoshimura	Aoi & Iwaki	Nagano	Hayakawa	Citak, Matsushima and Graves	Onishi
Grid space(m) or element size (m)	homogeneous(N11)		200/3	same as N12 ～N22	100	100	100	100
	two-layered (N12～N22)	upper lyaer	100/3	100/3	50	50	50	50
		lower layer	200/3	100	100	horizontal 50 vertical 100	50	horizontal 50 vertical 100
Choice of material property at the grid on the boundry of upper and lower layer			−	upper	averave	lower	averave	lower
Time increment(s)			0.002	0.0025	0.005(N11) 0.004(N12～N22)	0.005	0.005(N11) 0.025(N12～N22)	0.005
Division size of extended fault (m)			200/3	100	50	100	50	100

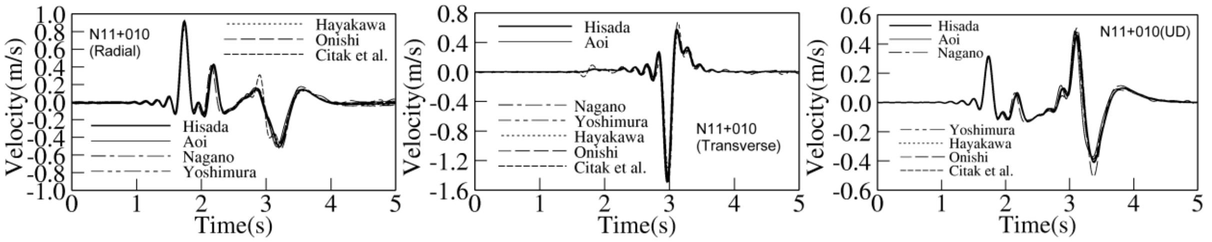

Figure 2. Velocity waveforms of N11 at +010. (a)Radial, (b)Transverse, (c)Up component.

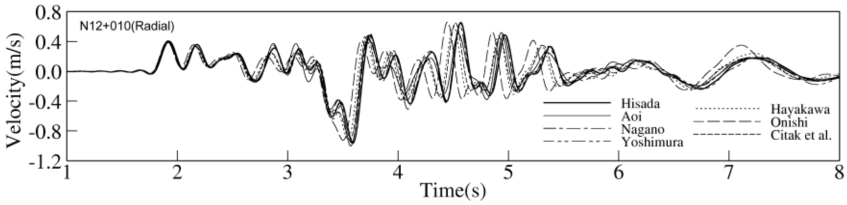

Figure 3. Velocity waveform of N12 at +010 (Radial component)

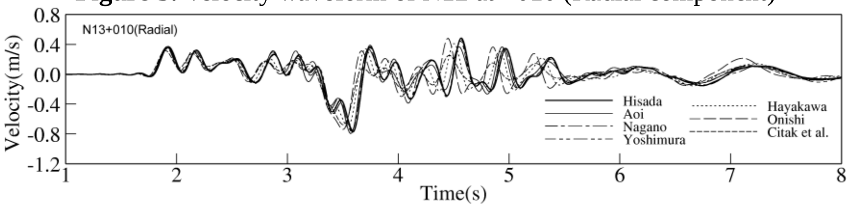

Figure 4. Velocity waveform of N13 at +010 (Radial component)

For N21, a vertical lateral fault shown in figure 1(c) is considered. Fault length is 8 km, fault width is 4 km, and mechanism is (strike, dip, rake)=(90, 90, 180)(deg). The rupture propagates concentrically from the initial rupture point, or hypocenter H(Hx, Hy, Hz)=(0, 1, 4)(km) with the rupture velocity of V_{rup}=3km/s. Slip function at a point (X, Y, Z) is given by eq. (3),(4),(5) and (6).

$$S(X,Y,Z,t)=S_0\left[1-(1+\frac{\tau}{T})e^{-\frac{\tau}{T}}\right] \quad (\tau \geqq 0) \qquad \ldots(3)$$

$$\tau = t-\xi/V_{rup} \qquad \ldots(4)$$

$$\xi=\sqrt{(X-H_x)^2+(Y-H_y)^2+(Z-H_z)^2} \qquad \ldots(5)$$

$$S_0 = 1(\mathrm{m}),\ T = 0.1(\mathrm{s}) \qquad \ldots(6)$$

For N22, a reverse fault shown in figure 1(d) is considered. Fault length is 4km, fault width is 4km and mechanism is (strike, dip, rake)=(115, 40, 70)(deg). Hypocenter is H(Hx, Hy, Hz)=(0, 0, 6)(km) and rupture velocity is V_{rup}=3km/s.

Figure 5 shows the results of N21. Transverse components at point -010, +002 and +010 (shown in fig. 1(c)) are compared. The point -010 is located at backward side of the rupture propagation, and +010 is forward side. The point +002 is above the fault. Similarly, figure 6 shows the results of N22 in the same manner. The results of all teams show good agreement to each other.

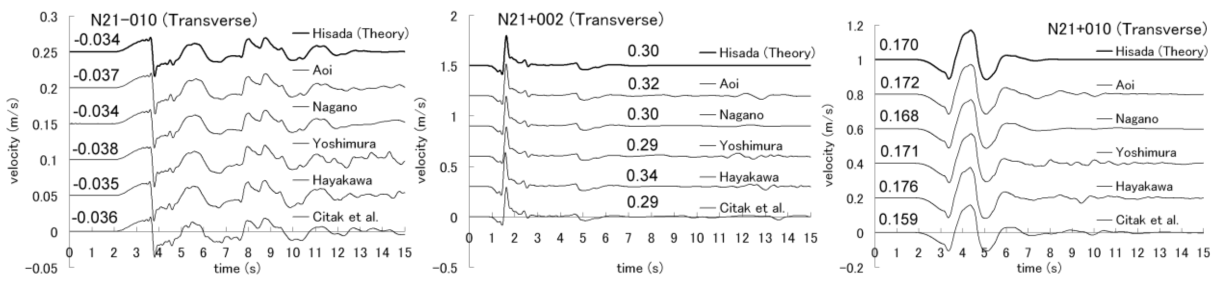

Figure 5. Transverse velocity waveforms of N21 at -010, +002, +010 (Numbers are peak amplitude)

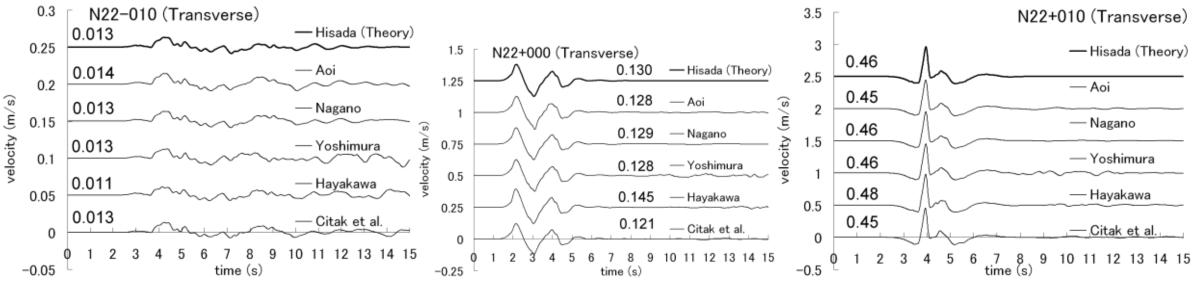

Figure 6. Transverse velocity waveforms of N22 at -010, +002, +010 (Numbers are peak amplitude)

3. STEP3, 4 (FOUR LAYERED MEDIA, IDEALIZED BASIN MODELS)

Table 5 summarizes 5 models studied in Step 3 and 4. We studied 4-layerd media for N31 and N32 examining the accuracy when engineering basement (Vs=400m/s) is considered for the upmost layer. The results ware as good as 2-layerd media (Figure are left out hear due to limitation of space). We considered a trapezoidal basin structure for N33 and an asymmetric slant-basement basin for N 41 and N42. Table 6 shows material properties. S wave velocity of sedimentary basin is Vs=1000m/s and that of basement is 3464 m/s. Q values are given to be proportional to frequency f(Hz). Figure 7 shows the subsurface structure models. Calculation domain is 30km x 30 km x 17 km and absorbing zone more than 2 km in thickness should be added at the model sides and the bottom. The shape of basin-basement boundary for N33 is given following Uebayashi et al.(1989). The flat part of the bottom is Lx=Ly=8km, the width of cosine-shape slope is Vx=Vy=2.4km, the total width of the basin at the surface is Lx+2Vx=Ly+2Vy=12.8 km and the thickness is 1km.

Point source C is located at under the south-western corner of the basin with the depth of 3km, or (X, Y, Z)=(-6.4, -6.4, 3)(km). Source mechanism is (strike, dip, rake)=(45, 90, 90)(deg), which corresponds to a vertical fault with vertical dislocation. Moment magnitude is set to be Mo=10^{18} Nm. Moment rate function and Moment function are given by eq (7), (8) respectively.

$$\dot{M}(t) = M_0 \bullet \frac{1}{\sqrt{2\pi}\sigma} \bullet \exp\left(-\frac{(t-\mu)^2}{2\sigma^2}\right) \qquad \cdots(7)$$

$$M(t) = M_0 \bullet \frac{1}{2}\left(1 + erf\left(\frac{t-\mu}{\sqrt{2}\sigma}\right)\right) \qquad \ldots(8)$$

Table 5. Test cases of Step 3 and 4

	Step3			Step4	
Case	N31	N32	N33	N41	N42
Media	four-layered media		trapezoidal basin	slant basement basin	
Internal damping	YES				
Source	point source				
Effective frequency	0 – 2.5 Hz				
calculation points	21	19	21	21	21

Table 6. Material properties

	P wave velocity Vp (m/s)	S wave velocity Vs (m/s)	Density ρ (kg/m^3)	Q Value Qp	Qs
Sedimentary basin	2600	1000	2400	30f	30f
Bedrock	6000	3464	2700	70f	70f

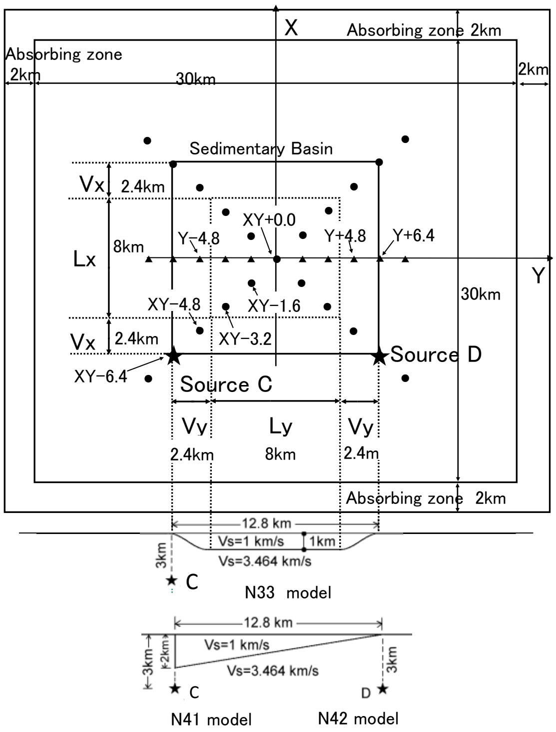

Figure 7. Plan and sections of basins of N33, N41,N42

Where t denotes time(s), σ=0.2(s), μ=4σ=0.8(s) and $erf(x)$ is the error function. We used Gaussian type function in step 3, 4 because the exponent type used in step 1 and 2 tends to generate high frequency noise due to rapid rise of M(t).

For N41, we considered a slant-basement basin, which is located at as the same horizontal position as N33. The basement falls off vertically to the depth of 2km at the western edge and becomes shallower towards east. The point source C same as that of N33 is considered. For N42, we considered the same subsurface structure and point source D whose mechanism is (strike, dip, rake)=(-45, 90, 90) (deg).

Figure 10 shows velocity waveforms of X, Y and Z components at the center (XY+0.0 shown in fig.7). Since there is no exact solution, Nagano's solution is compared to each team's solution as a reference. It can be said that all teams obtained almost consistent result for practical use. In detail, Yoshimura, Nagano and Aoi showed very good agreement to each other. On the other hand, slight differences are observed at surface waves that are dominant at 10s and after. Because of symmetry, Z component along X=Y line is expected to be zero. In figure (c), those results are nearly zero. It means that the results of all team's code have good accuracy.

Figure 9 shows X components at other points. Figure (a) shows those at XY-6.4 which is just above the source and at the boundary of sedimentary basin and basement. Figure (b) shows those at Y-4.8 which is above the source-side slope. In both figures, body waves are dominant and the results of all teams show good agreement to each other. Figure (c) shows the results at Y+4.8 which is above the slope opposite to the source. Around 15 second, surface waves induced near the source-side slope arrive. Each team's results show good agreement to each other except that Citak's result shows slight difference due to difference of implementation of Q.

In past years, boundary methods such as boundary element method or Aki-Larner method were often used. From the viewpoint of comparison to boundary method, Uebayashi solved N33 with AL method and compare to the results solved by Kawabe's FDM (σ is set to be 0.4 in eq.(7)(8)). Figure 10 shows the X components at five points along X=Y line. At the part before 13 seconds, both methods show good agreement. The results of AL method show arrival of large phase at 13 seconds and after. Because AL method solves spatially periodical structure including media and source, the large phase is due to the effect of neighbor source (rapround effect). If we chose larger spatial period, we can make the arrival of rapround effect delay.

Figure 11 shows results of N41. Velocity waveforms of X component at 3 points along X=0 are shown. Around 4 seconds of (a)Y-4.8, the peaks of S waves are obviously seen. Around 14 seconds of (b)Y+4.8, basin induced surface waves are recognized. All teams show good agreement to each other except Citak whose Q is differ from others. Figure 12 shows the results of N42. Velocity waveforms of X component at 3 points along X=0 are shown. The source D is located at opposite side of source C for N41. At (c)Y+6.4 which is on the boundary between basin and outcrop basement and is close to the source, short pulses of body waves are dominant. The results of all teams for these body waves show good agreement to each other. At (b)XY+0.0 which is center of the model and (c)Y=-4.8 which is far from the source, surface waves are dominant. The arrival time of the surface waves slightly varies among teams.

4. STEP5,6 (KANTO BASIN MODEL)

In Step5 and 6, we considered a 3-dimensional Kanto basin model and the source models of 4 observed earthquakes. Table 7 shows the calculation conditions. Figure 13 shows the calculation domain (210km x 270km) with source model (stars or circles) and 19 calculation sites. Grid space or element sizes were chosen so that the results is valid up to 0.33Hz (3 seconds). Subsurface structure mode1 were made based on the 20 layered model proposed in the project of "Long Period Ground

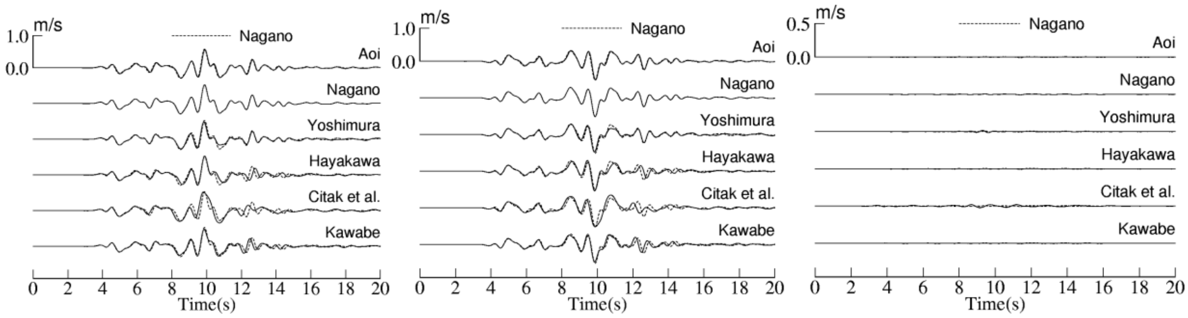

(a)X component (b)Y component (c)Z component

Figure 8. Velocity waveforms of N33 at XY+0.0

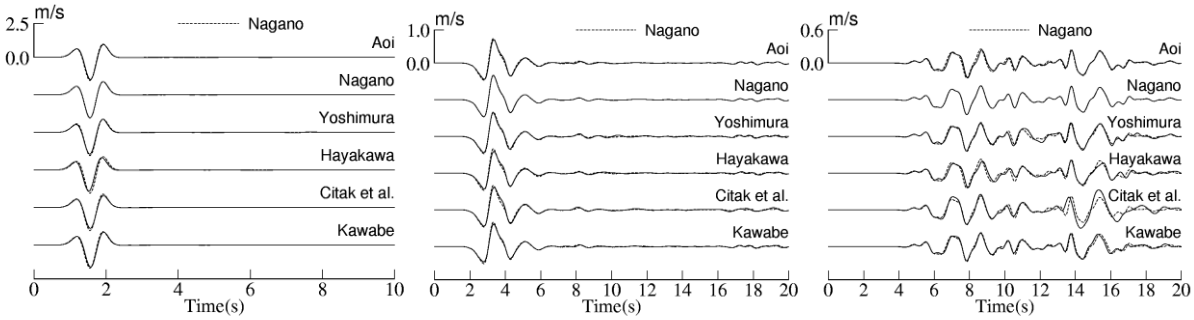

(a)XY-6.4 (b)Y-4.8 (c)Y+4.8

Figure 9. Velocity waveforms of X component of N33

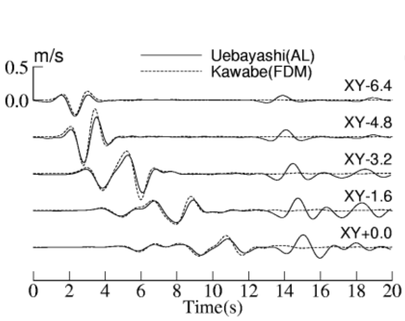

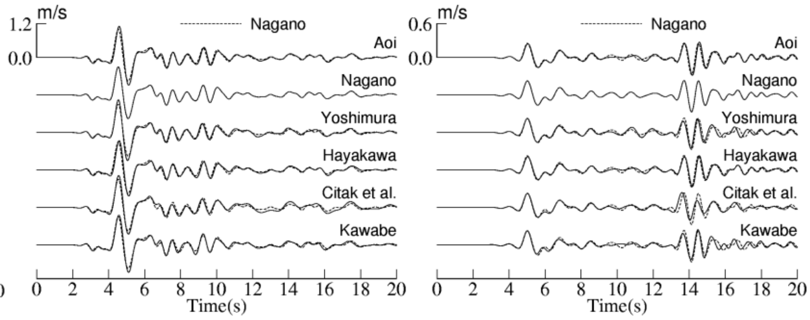

Figure 10. Comparison of AL method and FDM

(a)Y-4.8 (c)Y+4.8

Figure 11. Velocity waveforms of X component of N41

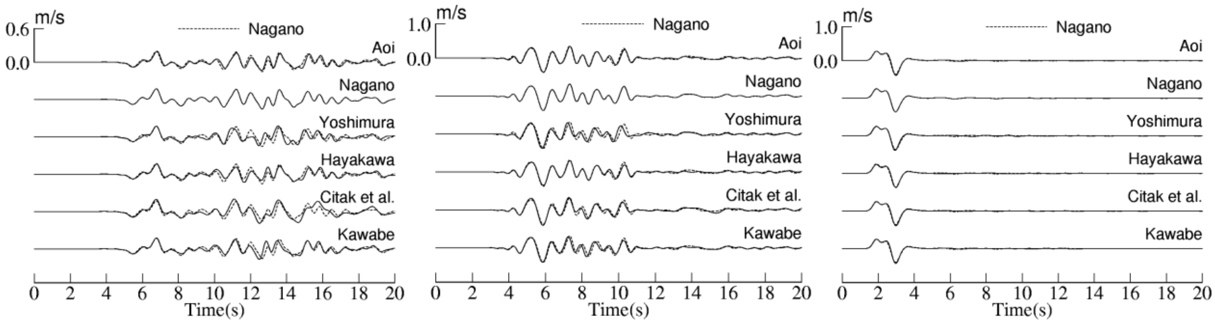

(a)Y-4.8 (b)XY+0.0 (c)Y+6.4

Figure 12. Velocity waveforms of X component of N41

Motion Prediction Map" by The Headquarters for Earthquake Research Promotion. Digital data of layer boundaries were distributed to the participants. Each participant allocated soil properties to grids or elements judging from vertical relation to boundaries.

In step 5, we targeted 3 small or middle earthquakes. Case N51 is for 1990 Western Kanagawa Prefecture earthquake (Mj 5.1), N52 for 1990 Near Izu-Oshima earthquake (Mj6.5) and N53 for 1992 Tokyo bay earthquake (Mj 5.7). N54 is an additional case where we recalculate N51 making the calculation condition such as grid space and allocation of material properties as same as possible because they varied among participants in N51. We constructed the source models based on Sato T. et al. (1998) and Yamada and Yamanaka (2003). In step 6, we targeted 1923 Kanto earthquake (Mj 7.9) for N61. The source model was constructed based on the inverted source model proposed by Sato H. et al. (2005). N62 is an additional case where we calculate with a homogeneous model (Vs=3.53 km/s) to assure that the source model of each participant is correct.

Figure 14(a) shows EW velocity waveforms at SMK of N51. The waveforms of initial body waves show good agreement among teams. On the other hand, those of the following surface waves vary. Regarding the grid space for N51, Citak selected 0.25km uniformly both in horizontal directions and in vertical direction. Iwaki & Aoi selected 0.3km uniformly in both directions. Nagano, Kawabe and Hayakawa selected 0.3km in horizontal directions, but their vertical grid space varied along depth. The vertical grid space of Nagano is 0.3km at the part shallower than 25.5 km. That of Kawabe is 0.3km at the part shallower than 3km and that of Hayakawa is 0.2 km at the part shallower than 3km. Yoshimura's FEM changed element size to be 0.15, 0.3, 0.6, 1.2 km in corresponding layers. Figure 15 shows vertical sections near SMK of Hayakawa (0.2km), Citak (0.25 and 0.3km) and Yoshimura(FEM). It shows that the allocation of soil properties near the surface vary depending grid space. In addition, Kawabe defined the soil property at the center depth of the grid space, that means, Kawabe's surface gird has the properties of those at 150m in depth. Other teams allocated the properties at 0m in depth to the surface grid. To amend above differences in calculation conditions, we carried out additional case N54. In that case, Citak and Kawabe recalculated N51 with uniform grids of 0.3km and Kawabe allocated soil properties in the same manner as other teams. Figure 14(b) shows the results of N54. The results of Citak and Kawabe approached other teams' results. In the same manner, figure 14(c) and 14(d) compare N51 and N54 at YKH(Yokohama). The degree of agreement of the following surface waves are improved in N54. Incidentally, Hisada's results with 1D model shows good agreement at the part of initial body waves, yet the following surface waves are inadequate. We can see the importance of 3D irregularity effect.

Figure 14(e) shows NS velocity component at JSK(Hongo) of N61 targeting 1923 Kanto earthquake. Some part of following surface waves differ among teams, they show generally good agreement to each other. However, the amplitude is much larger than observed records. This is because the source model was inverted with teleseismic waves and is roughly discretized about 10 km grid. To estimate strong motion in close distance, it is needed to set the division size of source model to be much smaller. Figure 14(f) shows the results of N62 where we recalculated N61 with homogeneous media to assure that each team's source model is correct. The waveforms of all teams show very good agreement to each other. It means that slight differences recognized in N61 and N54 are caused by remaining differences of subsurface structure.

Table 7. Test cases of Step 5 and 6

	Step 5				Step6	
Case	N51	N52	N53	(N54)	N61	(N62)
Earhquake	Kanagawa-ken seibu	Near Izu Oshima	Tokyo bay	retry of N51	1923 Kanto	source check of N61
Subsurface model	3D model of Kanto basin					
Source	point source	extended source	point source	point source	extended source	
Effective frequency	0 – 0.33 Hz					
calculation points	19					

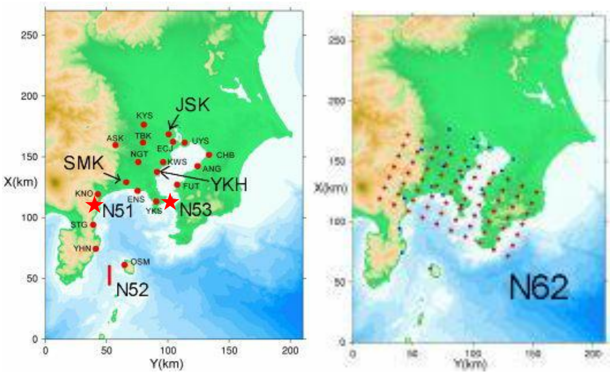

Figure 13. Source model and calculation points

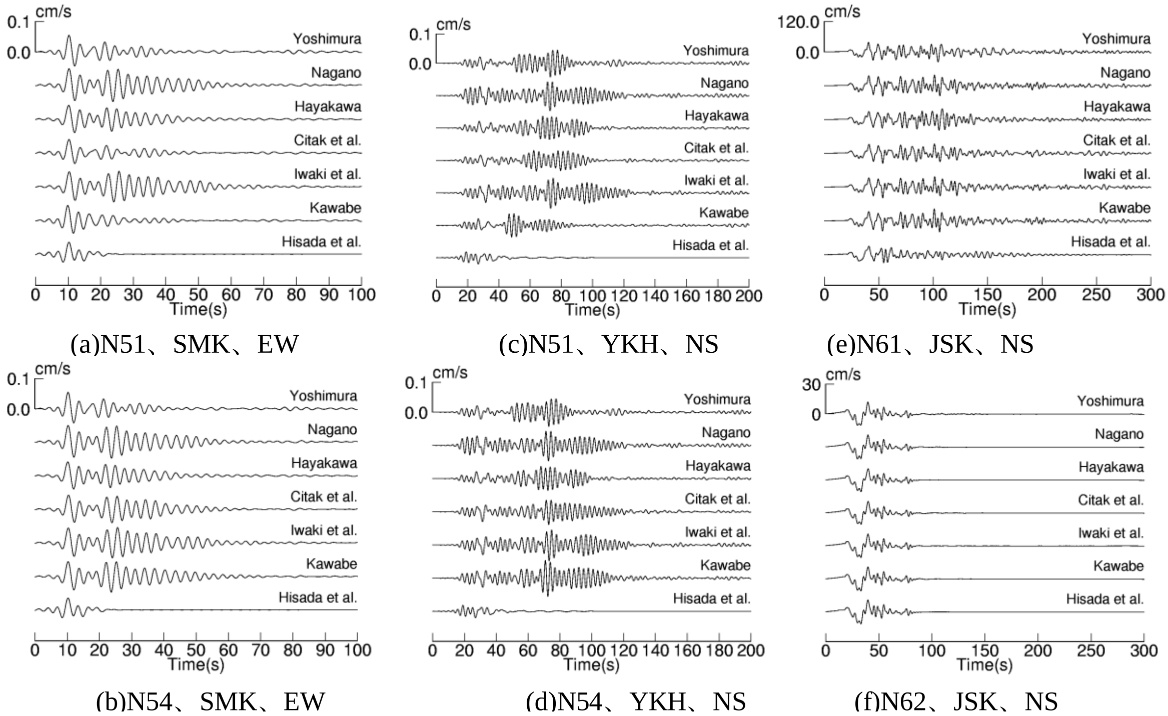

Figure 14. Results of N 51, N54, N61 and N62

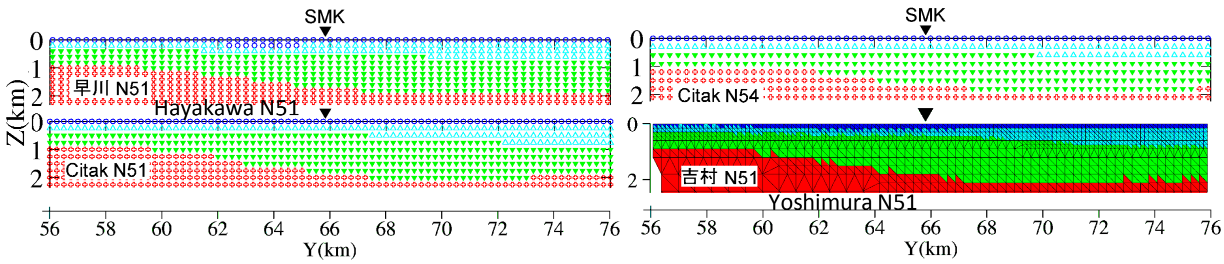

Figure 15. Vertical sections along EW direction around SMK

5. CONCLUSION

1) The results of 7 teams (one FEM team and 6 FDM teams) showed generally good agreement to each other with adequate accuracy for practical use.
2) The agreement of body waves was very good. Differences were found at the part of following surface waves.
3) The choice of soil properties at the grids on the boundary of surface layer and basement affects the results. Choosing basement properties makes phase velocity faster.

4) Choice of grid space makes differences of allocation of soil properties near the surface. It generates differences of waveforms.
5) Comparison with observed records in Step5 and recalculation with exactly same soil properties in Step 6 are remaining issues.

AKCNOWLEDGEMENT
This study is supported by Grant-in-Aid for Scientific Research (B) of The Ministry of Education, Culture, Sports, Science and Technology (MEXT) and is conducted in corporate with The Research Subcommittees on the Earthquake Ground Motion, The Architectural Institute of Japan and Research Center for Urban Disaster Mitigation, Kogakuin University. We appreciate Mr. Toshiaki Matsumoto and Dr. Robert W. Graves for partipating in the calculation. We would like to thank Dr. Toshiaki Sato, Dr. Nobuyuki Yamada and Dr. Reiji Kobayashi for providing us the source models.

REFERENCES

Aki, K. and P. G. Richards(2002). Quantitative Seismology Second Edition, p.50, University Science Books.
Aoi, S. and H. Fujiwara(1999). 3-D finite difference method using discontinuous grids, *Bull. Seism. Soc. Am.*, **89**, 918-930.
Architectual Institute of Japan(2009). Generation Guide for Seismic Input Motions Based on the Recent Advancement of Ground Motion Studies, Architectual Institute of Japan, Tokyo, Japan. (in Japanese)
Architectual Institute of Japan(2008). Seismic Loading – toward Performace Based Design, Architectual Institute of Japan, Tokyo, Japan. (in Japanese)
Bao, H., J. Bielak, O. Ghattas, L. F. Kallivokas, D. R. O'Hallaron, J. R. Shewchuk, and J. Xu(1998). Large-scale simulation of elastic wave propagation in heterogeneous media on parallel computers, *Comput. Methods Appl. Mech. Engrg.*, **152**, 85-102.
Clayton, R. and B. Engquist(1977) . Absorbing boundary conditions for acoustic and elastic wave equations, *Bull. Seism. Soc. Am.*, **67**, 1529-1540.
Cerjan, C., D. Kosloff, R. Kosloff and M. Reshef(1985). A nonreflecting boundary condition for discrete acoustic and elastic wave equations, *Geophysics*, **50**, 705-708.
Day, S. M., J. Bielak, D. Dreger, S. Larsen, R. Graves, A. Pitarka, K. B. Olsen(2000). Tests of 3D Elastodynamic Codes, Final Report to Pacific Earthquake Engineering Research Center, Lifelines Program TASK 1A01, 1-24.
Day, S. M., J. Bielak, D. Dreger, S. Larsen, R. Graves, A. Pitarka, K. B. Olsen(2003), Tests of 3D Elastodynamic Codes, Final Report to Pacific Earthquake Engineering Research Center, Lifelines Program TASK 1A02, 1-32.
Nagano, M.(2004). Evaluation of Strong Ground Motions in Kobe Area during The 2000 Tottori-ken Seibu Earthquake Using 3D Finite Difference Method with Variable Spacing and Time Increment. *J. Struct. Constr. Eng., AIJ*, **580**, 43-50. (in Japanese)
Pitarka, A.(1999). 3D Elastic Finite-Differences Modeling of Seismic Motion Using Staggered Grids with Nonuniform Spacing, *Bull. Seism. Soc. Am.*, **89:1**, 54-68.
Graves, R.(1996). Simulating Seismic Wave Propagation in 3D Elastic Media Using Staggered-Grid Finite Differences, *Bull. Seism. Soc. Am.*, **86:4**,1091-1106.
Graves, R. and S. Day(2003), Stability and Accuracy Analysis of Coarse-Grain Viscoelastic Simulations, *Bull. Seism. Soc. Am.*, **93:1**, 283–300.
Hisada, Y.(1994). An Effective Method for Computing Green's Function for a Layered Half-Space with Source and Receivers at Close Depth, *Bull. Seism. Soc. Am.* , 84:5, 1456-1472.
Hisada, Y.(1994). An Effective Method for Computing Green's Function for a Layered Half-Space with Source and Receivers at Close Depth (Part2), *Bull. Seism. Soc. Am.* , 85:4, 1080-1093.
Uebayashi H., M. Horike and Y. Takeuchi(1992). Seismic motion in a three-dimensional arbitarily-shaped sedimentary basin, due to a rectangular dislocation source, *J. Phys. Earth*, **40**, 223-240.
Uebayashi H., M. Horike and Y. Takeuchi(1989). Seismic Response of a Three-dimensional Sedimentary Basin with an Irregular Interface to a Rectangular Dislocation Source in a Half-Space, AIJ Kinki Branch 1989 Research Report, 65-68. (in Japanese)
Yoshimura, C. et al.(2011). Benchmark tests for strong ground motion prediction methods: Case for Numerical Methods (Part 1). *AIJ J. Technol. Des.* **Vol. 17:No.35**, 67-72. (in Japanese)
Yoshimura, C. et al.(2012). Benchmark tests for strong ground motion prediction methods: Case for Numerical Methods (Part 2). *AIJ J. Technol. Des.* **Vol. 18:No.38**, 95-100. (in Japanese)